

Supporting Information

Strongly Coupled Plasmonic Modes on Macroscopic Areas via Template-Assisted Colloidal Self- Assembly

*Christoph Hanske,[†] Moritz Tebbe,[†] Christian Kuttner,[†] Vera Bieber,[†] Vladimir V. Tsukruk,[‡]
Munish Chanana,^{†,§} Tobias A. F. König,^{*,†,‡} and Andreas Fery^{*,†}*

[†]Physical Chemistry II, University of Bayreuth, Universitätsstraße 30, 95440 Bayreuth, Germany

[‡]School of Materials Science and Engineering, Georgia Institute of Technology, Atlanta,
Georgia 30332-0245, United States

[§]Institute of Building Materials (IfB), ETH Zürich, Stefano-Franscini-Platz 3, 8093 Zürich,
Switzerland

Corresponding Authors

* E-mail: (T.K.) tobias.koenig@uni-bayreuth.de

* E-mail: (A.F.) andreas.fery@uni-bayreuth.de

The following section explains the experimental procedures utilized for the fabrication and characterization of the nanoparticle chains and contains information about the conducted FDTD and GMMT simulations.

Additionally, we provide characterization of the gold nanoparticles, AFM images of the wrinkled PDMS templates prior to particle transfer, measured and simulated spectra of isolated particles, FDTD/GMMT simulations of dimers and chains as well as spectra modeled with and without periodic boundary conditions.

MATERIALS & METHODS

Chemicals

Deionized water was purified with a Milli-Q system (Millipore). Ready-made HCl and NaOH solutions (1 M, Grüssing) were utilized to adjust the pH. For the synthesis of the gold nanoparticles, analytical grade chemicals were used without further purification. Citrate (99%, Grüssing), sodium borohydride (NaBH_4 , 99.99%, Sigma-Aldrich), gold(III) chloride trihydrate ($\text{HAuCl}_4 \cdot 3\text{H}_2\text{O}$, 99.9%, Sigma-Aldrich), cetyltrimethylammonium bromide (CTAB, 99%, Merck), ascorbic acid (99.5%, Grüssing), and bovine serum albumin (BSA, 98%, Sigma-Aldrich) were used as received. To avoid bacterial contamination, citrate buffered BSA solutions were freshly prepared before the protein coating of the gold nanoparticles. Polydimethylsiloxane elastomer kits (PDMS, Sylgard 184) were purchased from Dow Corning. Quartz substrates (Electron Microscopy Sciences) were cleaned with analytical grade isopropanol (VWR) and coated with branched polyethylene imine (PEI, $M_w = 25$ kg/mol, Sigma-Aldrich).

Particle Synthesis and Surface Modification

Gold nanoparticles were produced via a modification of the well-established two step seed-mediated synthesis procedure developed by Jana *et al.*¹⁻³ Briefly, citrate-stabilized seed particles with a typical diameter of 3.5 nm were prepared by adding 600 μL of a 0.1 M NaBH_4 solution to 20 mL of an aqueous 0.25 mM HAuCl_4 solution, stabilized with 0.25 mM sodium citrate, stirred at 1200 rpm for 2 min followed by 45 min of aging without stirring. 480 μL of the as-prepared seeds were added to a 0.1 M aqueous CTAB growth solution containing 0.5 mM HAuCl_4 and 7.5 mM ascorbic acid as reducing agent. The particle growth took place over 24 h at 32 °C yielding quasi-spherical Au particles with an average diameter of 78 nm (standard deviation:

4 nm, size determination by TEM) stabilized by a CTAB double layer. For storage, the CTAB concentration was kept at 0.1 M. The amount of nonspherical byproducts such as rods and plates was effectively reduced to a minimum by keeping the suspension at 32 °C for several days and subsequent removal of the brown sediment. Prior to the protein coating, the CTAB concentration was reduced below 1 mM by centrifugal washing at 2000 rcf while increasing the nanoparticle concentration by a factor of 10.

The BSA coating was conducted following a slightly modified procedure reported by Strozyk *et al.*⁴ To 25 ml of a BSA solution (10 mg/mL, citrate-buffered with 0.2 mg/mL), 5 mL of the gold nanoparticles suspension were added dropwise while shaking the flask. Directly after mixing and short sonication, the suspensions were centrifuged at 2000 rcf for 15 min. Precipitation of the particles on the walls of the centrifuge tubes allowed an easy exchange of the supernatant with fresh BSA solution (1 mg/mL, pH 11-12) followed by redispersion via sonication. The suspensions were stored in the fridge overnight and then cleaned by multiple centrifuge washing steps with alkaline water (pH 9). Highly concentrated stock solutions of the protein-coated particles (Au(0) in water: 15 mg/mL) were stable at pH 9 for several months. Further details on the particle properties are provided in Figure S1 and S2.

Particle Characterization

Extinction spectra of diluted gold nanoparticle suspensions were measured with a SPECORD PLUS 250 (Jena Analytik) spectrometer using quartz cuvettes (Hellma Suprasil). The zeta potential of BSA-coated particles was probed for pH values between 3 and 12 with a Zetasizer Nano-ZS (Malvern) system. Samples for transmission electron microscopy (TEM) were prepared by applying 2 μ L of a dilute particle suspension to a freshly hydrophilized carbon-coated copper grid and removing the excess suspension after 60 s by blotting with filter paper. Imaging was

performed with a Zeiss EM922 OMEGA EFTEM (Zeiss NTS GmbH) equipped with an UltraScan 1000 CCD camera (Gatan). The measurements were conducted at room temperature with an acceleration voltage of 200 kV.

Wrinkled Templates

The PDMS elastomer was prepared by mixing precursor polymer and hardener at a ratio of 10:1, degassing, and casting into a leveled petri dish. After gelation at room temperature for one day, the PDMS was cured at 80 °C for 5 h. Stripes with a width of 1 cm and a length of 4 cm were cut out of the resulting 2 mm thick elastomer plate. To remove dust, the stripes were shortly rinsed with deionized water and blown dry in a nitrogen stream. Subsequently, the stripes were fixed in custom-built stretching stages, strained by varying degrees, and treated with oxygen plasma (O₂ pressure: 0.2 mbar, 100 W power). During the treatment process, a thin glass-like layer with a stiffness exceeding that of the elastomeric substrate by several orders of magnitude is formed. Upon strain release, the PMDS stripes return to almost their original length, and the mechanical mismatch between the two layers causes buckling instabilities.⁵ In the case of uniaxial elongation, well-defined 1-dimensional surface corrugations with a sinusoidal cross-sectional profile arise. Hereby, the thickness of the glass-like layer is adjusted by the plasma dose and the preset strain can be utilized to tailor the geometry of the resulting surface wrinkles. The exact values of strain ϵ , treatment time t , and corresponding wrinkle wavelength λ are listed in the following table (Table S1).

Table S1: Preparation parameters of the employed PDMS templates.

PDMS template	ϵ in %	t in min	λ in nm
Wrinkle-1	40	3	360
Wrinkle-2	15	10	770
Wrinkle-3	15	15	1060

Particle Assembly and Transfer

The corrugated PDMS stamps can be used as templates for arranging nanoparticles into close-packed linear assemblies via spin coating. As long as the height of the wrinkles is comparable to the particle diameter or slightly larger, adjustment of the wavelength presents a reliable method for tuning the geometry of the resulting particle chains. With the chosen parameters single particle, dimer, and tetramer chains are accessible. Directly before spin coating, the wrinkled templates were cut into pieces of 1x1 cm² and rehydrophilized in the plasma etcher (Flecto 10, Plasma Technology) for 1-2 min. Onto each PDMS template 3 μ L of concentrated nanoparticle suspension (Au content: 10 mg/mL, adjusted to pH 11) were applied. After spreading, the spin coater (Photo-Resist Spinner, Headway Research Inc.) was started with a low acceleration. The characteristic red color of the suspension turned into a grayish tint after approximately 30 s of spinning at 1500-1800 rpm, indicating close contact between the Au nanoparticles. To prevent drying fringes forming near the corners of the PDMS stamps from reaching into the central regions, the rotational speed was subsequently increased to 3500 rpm for another 30 s. AFM images of various particle-filled templates are displayed in Figure S3.

The nanoparticle assemblies immobilized inside the grooves of the PDMS templates were then transferred onto flat substrates. For this purpose, polished quartz glass slides were cleaned by 10 min of sonication in isopropanol and 60 min of plasma treatment (0.2 mbar O₂, 100 W). To achieve a quantitative transfer of the protein-coated particles, an adhesion-promoting surface

layer on the target substrate was necessary. The freshly cleaned quartz pieces were immersed in PEI solutions (10 mg/mL) for at least 30 min, washed with deionized water, and dried in a nitrogen stream. For the transfer, 30 μ L droplets of water (pH 9) were placed on the PEI-coated quartz slides before the particle-filled PDMS stamps were pressed onto the target substrates with a pressure of approximately 100 kPa. The pressure was built up by a weight of 1 kg and was maintained during the entire transfer process. After 2 h the droplets had completely evaporated and the templating stamps could be removed leaving the nanoparticles chains on the adhesive target substrate.

Substrate Characterization

The nanoparticle assemblies on wrinkled PDMS stamps and flat substrates were imaged with a Nanoscope Dimension V (Bruker) atomic force microscope (AFM) operated in TappingMode™. Aluminum-coated silicon cantilevers (OTESPAW, Bruker) with typical resonance frequencies around 300 kHz and a specified stiffness in the range of 12 - 103 N/m were employed. All image processing and analysis was conducted in Gwyddion.⁶ For scanning electron microscopy (SEM), a LEO Gemini (Zeiss) system was used with acceleration voltages between 1 kV and 3 kV and a typical working distance of 4 mm. The samples were not sputter-coated in order to prevent alteration of the optical properties.

Optical Characterization of Nanoparticle Assemblies

All samples were thoroughly plasma-cleaned to remove organic residues, which might cause measurable shifts of the plasmon resonances due to local variations of the refractive index. Polarized far-field extinction spectra were measured with a commercial UV/vis/NIR spectrometer (V-670, Jasco) equipped with a film holder and a rotatable polarizer (GPH-506,

Jasco). All samples were mounted with the coated side facing toward the light source and the long axis of the nanoparticle chains in horizontal orientation. For the entire spectral range probed (400-2500 nm), a halogen lamp was employed as the light source. Between 400 and 900 nm the spectral bandwidth was set to 1 nm, whereas the NIR region was investigated with a bandwidth of 4 nm. These settings ensured that the same area of the sample surface was illuminated below and above the grating changeover located at 900 nm. The detector changeover from a PbS detector used in the NIR region to a photomultiplier tube for the UV/vis region coincided with this spectral position. For each sample, spectra were recorded with 11 different polarizer settings (0° to 90° in 10° steps, plus 45°). Background corrections were conducted with a set of spectra recorded with corresponding polarizer settings and a cleaned quartz glass slide as the blank sample.

FDTD Simulations

A commercial simulator based on the finite-difference time-domain (FDTD) method was used to perform the calculations of extinction spectra and surface charge distributions (Version 8.7.3, Lumerical Solutions Inc.). The gold refractive index data was adopted from Johnson and Christy.⁷ The simulation software fitted this material data with six coefficients and an RMS error of 0.211. A total-field scattered-field source was used and the frequency points were set to be half the wavelength span in nanometers. A simulation mesh size of either 1 nm or 0.5 nm was chosen to achieve an optimal balance between accuracy and simulation time. For the best simulation stability, the mesh area was chosen to be 60 nm larger than the existing structure in all three principal directions. All simulations reached the auto shut off level of 10^{-4} before reaching 200 fs of simulation time. The perfect match layer method was used for all boundaries. The zero conformal variant mesh refinement was utilized. To determine the surface charge density, we

simulated the model at the plasmonic mode frequency with a specific pulse length >20 fs using the optimization for long pulses.

GMMT Simulations

For ideally spherical particles the optical response can be modeled with strongly reduced computational effort using Mie theory.⁸ Analytic solutions for systems containing a finite number of spheres are obtained within the framework of the generalized multiparticle Mie theory (GMMT).⁹ For the GMMT calculations in this work, an algorithm developed by Yu-lin Xu¹⁰⁻¹² and Bo A. S. Gustafson¹³ as well as the extension GMMFIELD by Moritz Ringler^{14,15} were employed, using optical data by Johnson and Christy.⁷ GMMT simulated extinction spectra of single gold spheres coincided with corresponding FDTD simulations (see Figure S4 and S5), and also for the dimers excellent agreement was found between FDTD and GMMT simulations even though the latter were conducted without consideration of the substrate (see Figure S7). Consequently, GMMT was used for calculating the extinction, absorption, and scattering cross sections of all longer particle chains (single, dimer, and tetramer lines). The original code by Yu-lin Xu was modified and extended to allow for parallelized calculations employing the btrzx3 linux cluster (70 cores @ 2.8 GHz with 4 GB RAM in total) at the University of Bayreuth. The high resource-efficiency of the optimized code allowed us to screen a variety of particle configurations. The full ensemble of simulated spectra of nanoparticle assemblies in single particle, dimer, and tetramer chains (containing up to 120 particles at interparticle distances ranging from 1 nm to 10 nm) were obtained within 14 days of total calculation time.

Simulation of Gap Size Variations within Chains

GMMT was applied to study the influence of gap size variations on the longitudinal extinction spectra of nanoparticle chains. First, an ideal chain with uniform 1.5 nm gaps was simulated for a single particle line and a dimer line configuration. Second, an IGOR Pro procedure was used to assign variable gap sizes in the form of random values drawn from a uniform distribution within a range of [lower limit, upper limit]. The random number generator was initialized using the system clock when the program started. This practically guarantees that no identical sequence of gap sizes is drawn twice. That way, 20 spectra were simulated for each disordered chain morphology based on a variability in gap sizes of [1 nm; 1.5 nm], [1.5 nm; 2 nm], ... up to [1.5 nm; 10 nm]. Finally, the spectra were arithmetically averaged for each respective degree of disorder and compared to the experimental data. Figure 6 in the manuscript summarizes the simulated spectra and correlates the resulting shift of the mean superradiant mode $\langle\lambda_{\text{super}}\rangle$ with the corresponding mean interparticle distance $\langle\text{IPD}\rangle$. Equation S1 describes the resonance shift (see Table S2).

$$\langle\text{IPD}\rangle/\text{nm} = a + b \cdot (\langle\lambda_{\text{super}}\rangle/\text{nm})^c \quad \text{Eq. S1}$$

Table S2. Fitting coefficients for Eq. S1 describing the mean interparticle distance $\langle\text{IPD}\rangle$ as a function of the mean superradiant mode $\langle\lambda_{\text{super}}\rangle$ in the longitudinal extinction spectra of nanoparticle chains with randomized gap sizes.

	<i>a</i>	<i>b</i>	<i>c</i>	χ^2
single particle line (10x1)	0.329	9.9637e22	-7.8898	0.00845104
dimer line (10x2)	-0.795	3.328e13	-4.4113	0.0488725

SUPPORTING INFORMATION FIGURES

Particle Characterization

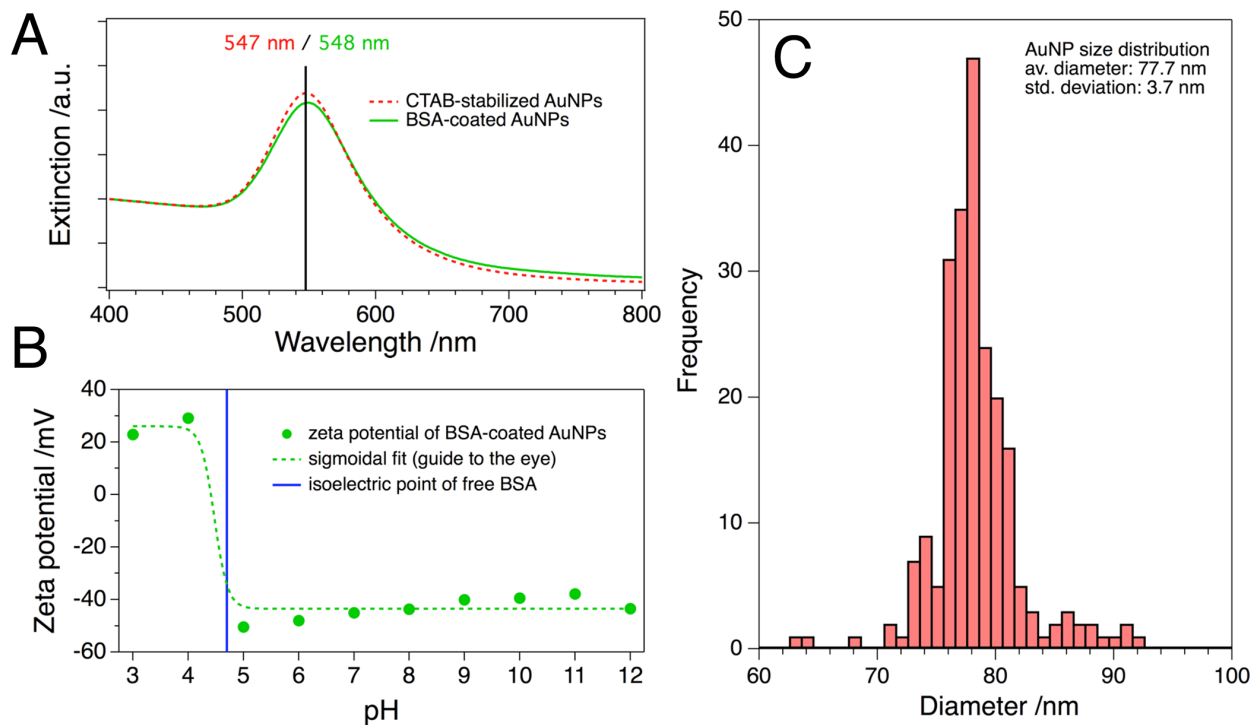


Figure S1. Single particle characterization: UV/vis spectra of Au nanoparticle suspensions measured before and after protein coating (A), pH-dependent zeta potential of BSA-coated Au nanoparticles (B), size distribution of the gold nanoparticle cores evaluated from TEM images (C).

TEM Images of Protein-coated Gold Nanoparticles

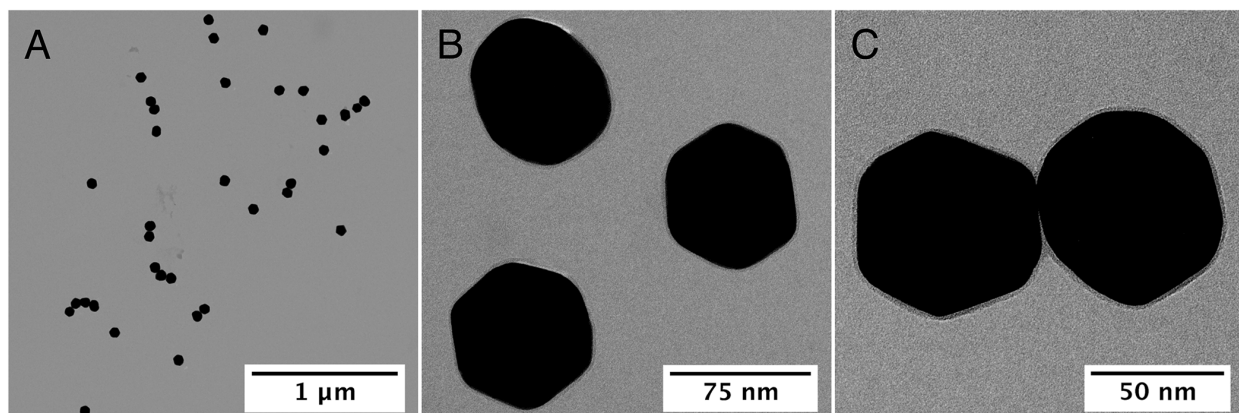


Figure S2. TEM micrographs of BSA-coated Au nanoparticles at various magnifications: the particles exhibit a narrow size distribution (A) and are coated with a thin, uniform protein shell (B). The soft coating is deformable and enables nanometer-sized interparticle distances in dried assemblies (C).

Spin-Coated Au Nanoparticle Assemblies on Wrinkled PDMS

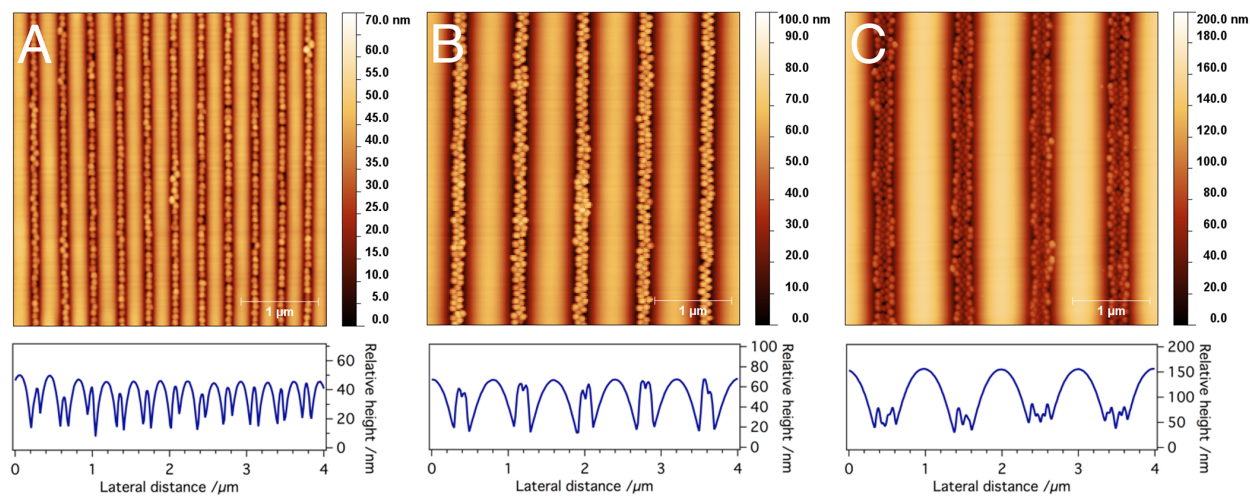


Figure S3. Gold nanoparticle assemblies on wrinkled PDMS stamps with corresponding cross sections below: with the wrinkling periodicity increasing from 360 nm (A) over 770 nm (B) to 1060 nm (C), a step-wise transition from single particle lines over dimer lines and finally to tetramer lines was observed. These particle assemblies were subsequently transferred onto quartz glass for further studies presented in the main paper.

Measured Spectrum of Randomly Deposited, Separate Particles and Comparison with Modeled Spectra of Single Particles on Quartz Substrates

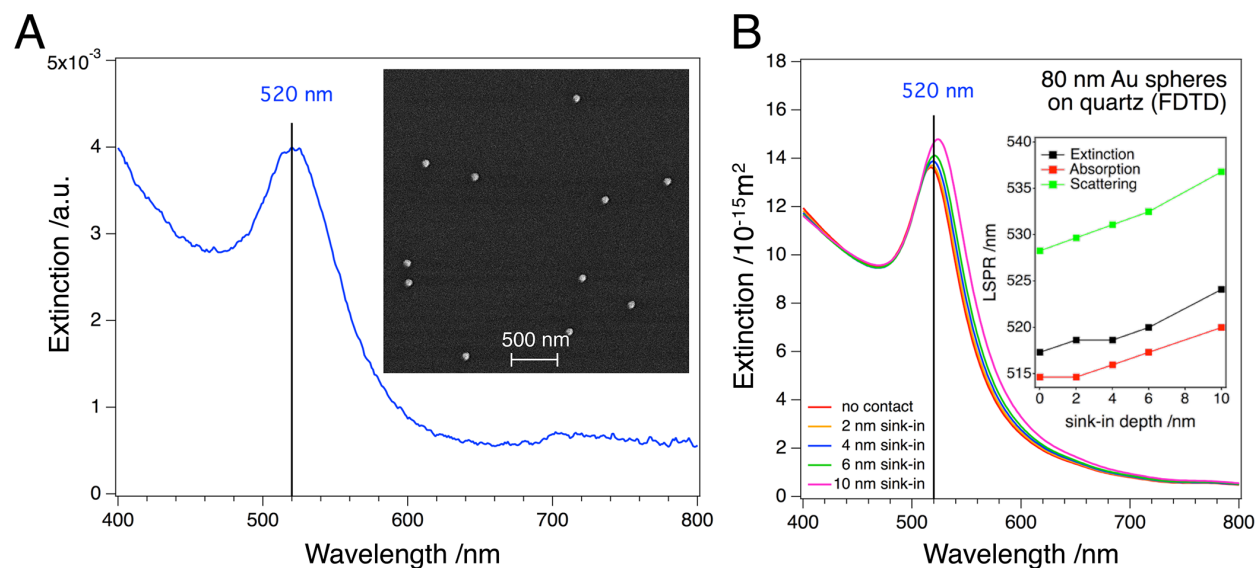


Figure S4. Extinction spectra of noncoupling, spherical Au nanoparticles: unpolarized vis-spectrum (A) of randomly adsorbed Au nanoparticles on quartz glass (measured in air after plasma cleaning). The inset shows a representative SEM image of the substrate. Extinction spectra (B) modeled by FDTD: the presence of the quartz substrate/residual protein (mimicked in the simulations by partial sinking into the substrate) causes a minor red shift of the single particle resonance compared to spectra simulated in absence of a substrate. Optimal agreement between the modeled and the measured LSPR position is found for a sink-in depth of 4 nm. The inset describes the LSPR position as obtained from the simulated extinction, absorption and scattering cross sections.

Simulations of Single Particle Spectra

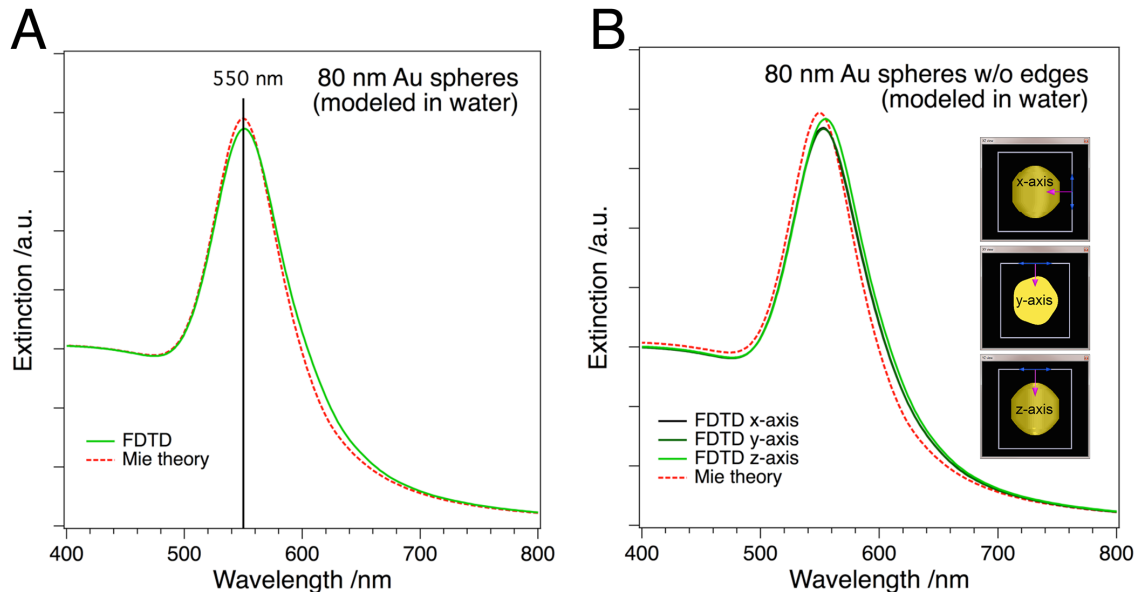


Figure S5. Simulations of gold nanoparticles in water via FDTD and Mie theory ($n=1.334$): with both methods the spectral response of the employed nanoparticles is described sufficiently by the approximation as ideal spheres with a diameter of 80 nm (A). The simulations correctly predict the measured resonance wavelength at 550 nm (experimental data included in Figure S1). Comparison of an ideal Au sphere (Mie theory) and a penta-twinned Au particle (FDTD) of the same size (B): accounting for their geometrical shape, the particles are exposed along the x-, y- and z-axis (magenta arrow indicates the wave vector) with vertical/horizontal polarization (blue double arrow) as shown in the inset schemes. The results for the x-, y-, and z-axis are the mean value of the vertical/horizontal polarization. The deviation between the averaged LSPR position obtained by FDTD ($\langle\lambda_R\rangle$) and Mie theory predictions is below 1% (i.e. 0.65%). Consequently, the approximation by spherical particles is valid, which also agrees very well with the experimentally observed spectral response of the employed nanoparticles. For the 80 nm penta-twinned particles, we assumed a corner rounding of 25 nm and a tip height of 25 nm, which are in good agreement with TEM observations and the typical results of the synthesis procedure.

Measured and Simulated Extinction Spectra of Single Particle and Dimer Chains

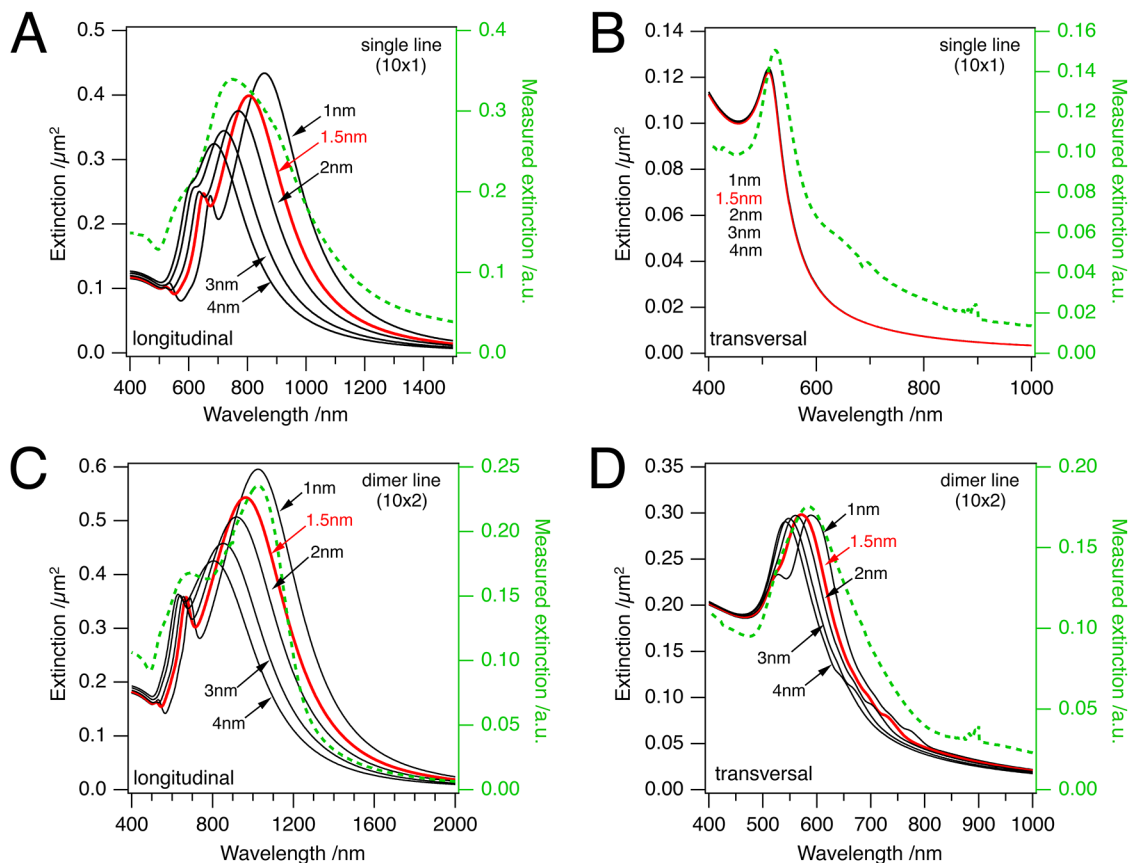


Figure S6. Comparison between measured extinction spectra (green) and GMMT simulations of single particle (A/B) and dimer (C/D) chains with 10 repeat units and varying interparticle distances (1, 1.5, 2, 3, and 4 nm): for both chain types the configurations with a constant gap size of 1.5 nm (red) deliver a good overall match. For this interparticle distance, the position of the energetically lowest peak in the longitudinal spectra (single particle lines: A, dimer lines: C) is sufficiently predicted. Besides the position of the superradiant coupling mode, the occurrence of higher order coupling modes can be regarded as a sensitive distance indicator. For the dimer lines a quadrupolar coupling mode near 530 nm is predicted if gaps smaller than 3 nm are employed in the simulations. This mode is visible in the spectra measured with longitudinal (C) as well as transversal (D) polarization.

Comparison of FDTD and GMMT Results for a Dimer of Coupling Particles

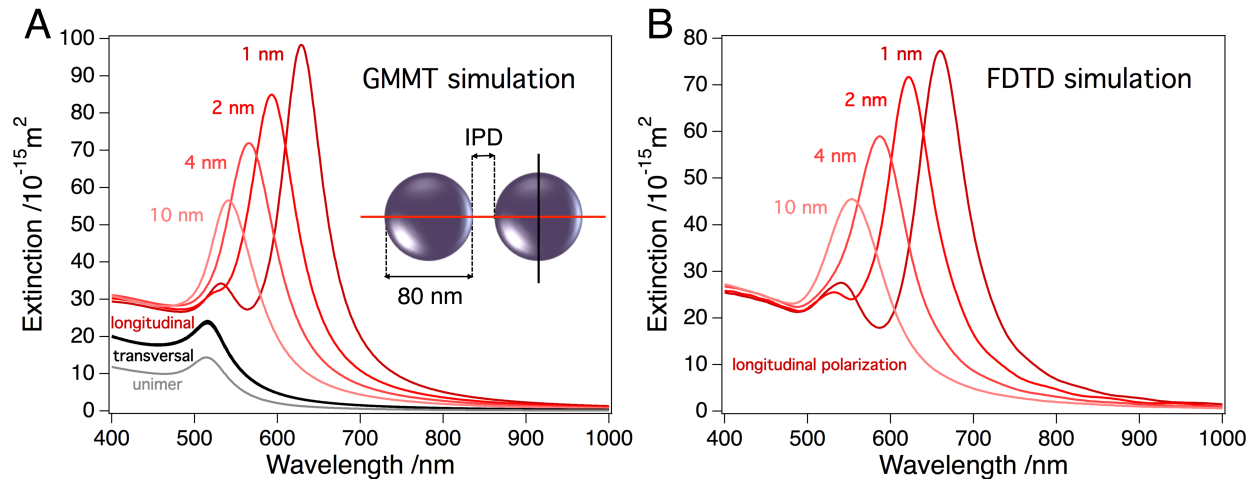


Figure S7. Comparison of spectra of a dimer of coupling particles simulated by GMMT (A) and FDTD (B): both methods are in excellent agreement showing comparable peak positions and shapes. The peak splitting for longitudinal coupling becomes clear in both methods only for an interparticle distance (IPD) as small as 2 nm where the dipolar coupling mode is sufficiently red shifted to reveal the presence of the higher order coupling mode.

FDTD Extinction Cross Section Simulations of a Gold Nanosphere Dimer

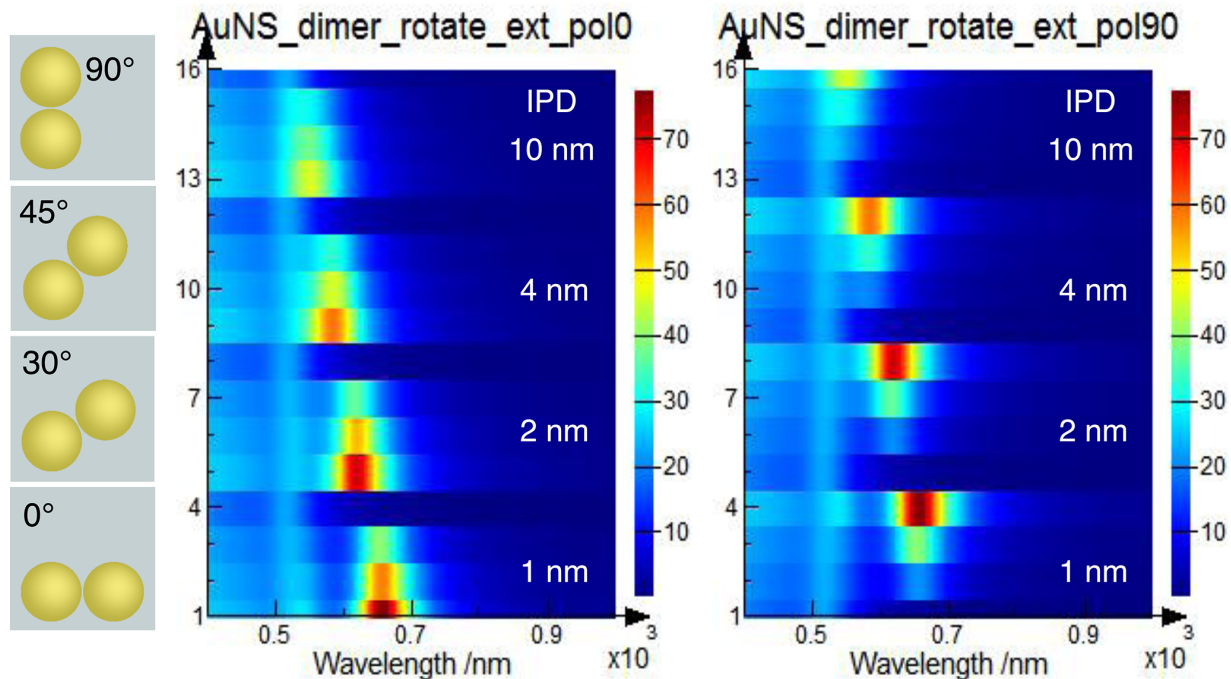


Figure S8. FDTD extinction cross section simulations of gold nanosphere dimers with interparticle distances (IPD) between 1 nm and 10 nm: each of the 4 sub-segments corresponds to a certain relative polarization angle (0°-90° from bottom to top). At small separations, orientations with a longitudinal polarization component show not only a dipolar but also a quadrupolar coupling mode (around 530 nm).

Extinction Cross Sections and Surface Charge Densities of a Gold Nanosphere Dimer at 0° and 30° Relative Rotation

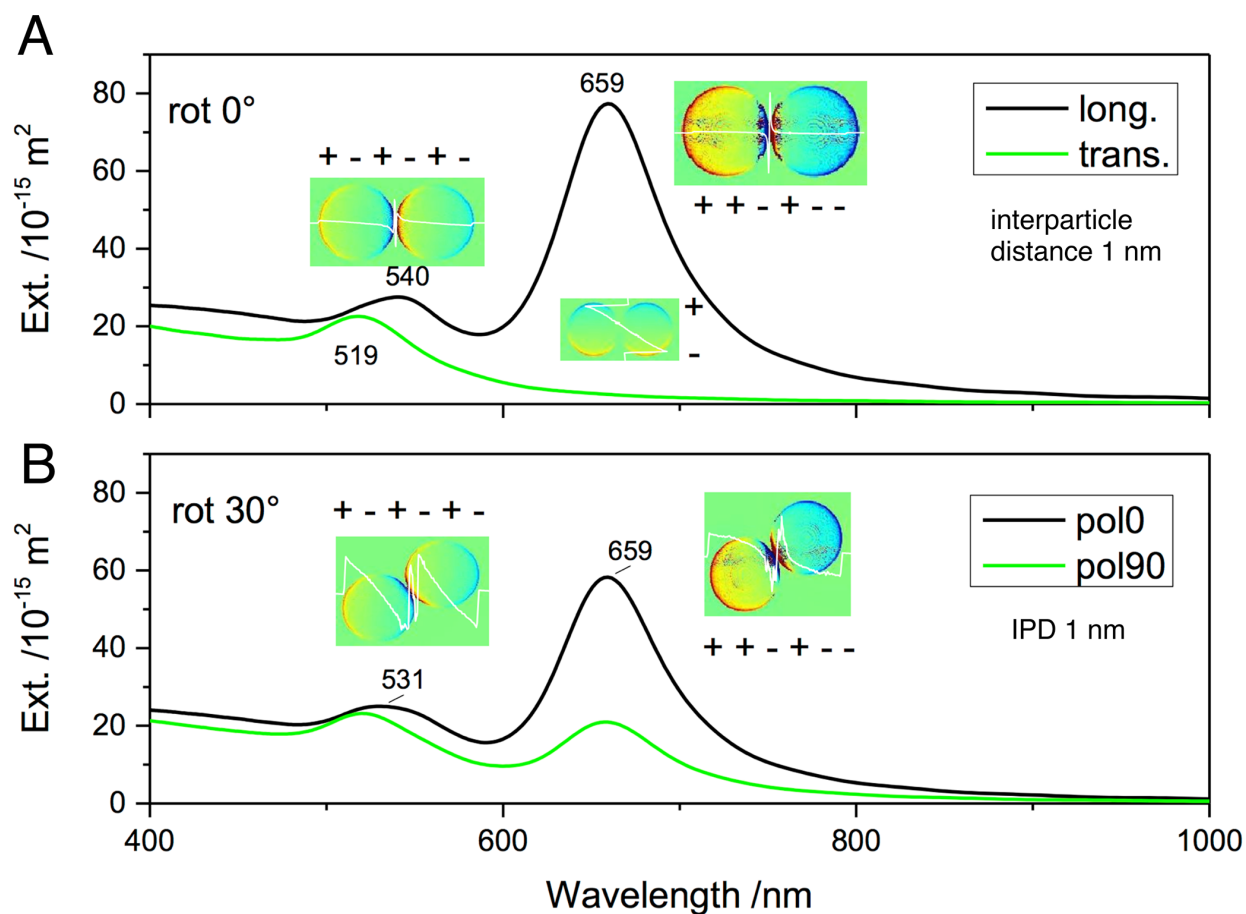


Figure S9. Extinction cross sections and surface charge densities of a dimer investigated at 0° and 30° relative rotation via FDTD: the dipolar mode excitation at lower energy and the quadrupolar mode excitation at higher energy are nearly independent from the relative rotation in this angular range. The plasmonic mode identification was based on an integration of the surface charge densities (white line). The color scales of the surface charge density plots were adjusted for improved clarity.

Influence of Defects on the Coupling between Neighboring Chains

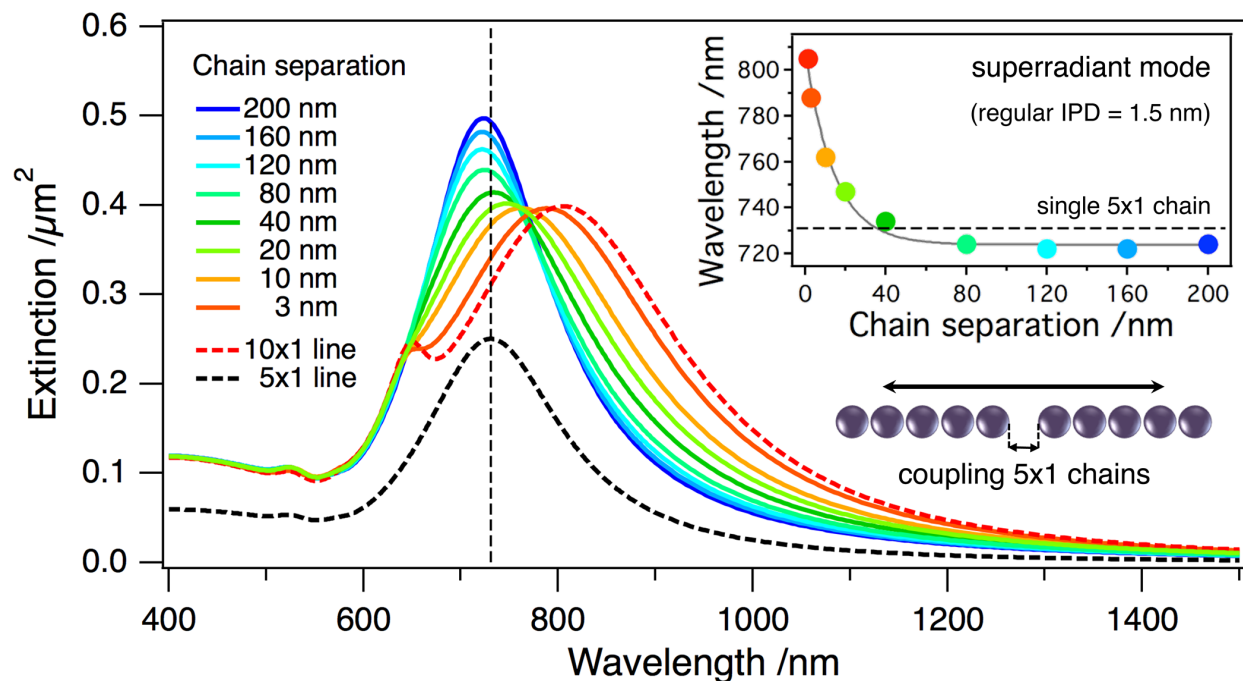


Figure S10. Longitudinal extinction spectra of nanoparticle chain pairs with different separations (5 particles per chain, modeled with an interparticle distance of 1.5 nm via GMMT): for fragments shorter than the “infinite chain limit”, the spectral position of the superradiant mode indicates the coupling strength. With increasing separation, the energetically lowest peak quickly shifts toward the blue. The inset shows that the position of this peak basically corresponds to the superradiant mode of isolated pentamer chains (dashed line) for gaps larger than 40 nm, i.e. one particle radius. For larger separations only weak coupling effects are observed. The exponential fit (gray line) serves as a guide to the eye.

2D Modeling of Grating Effects caused by Periodic Boundary Conditions

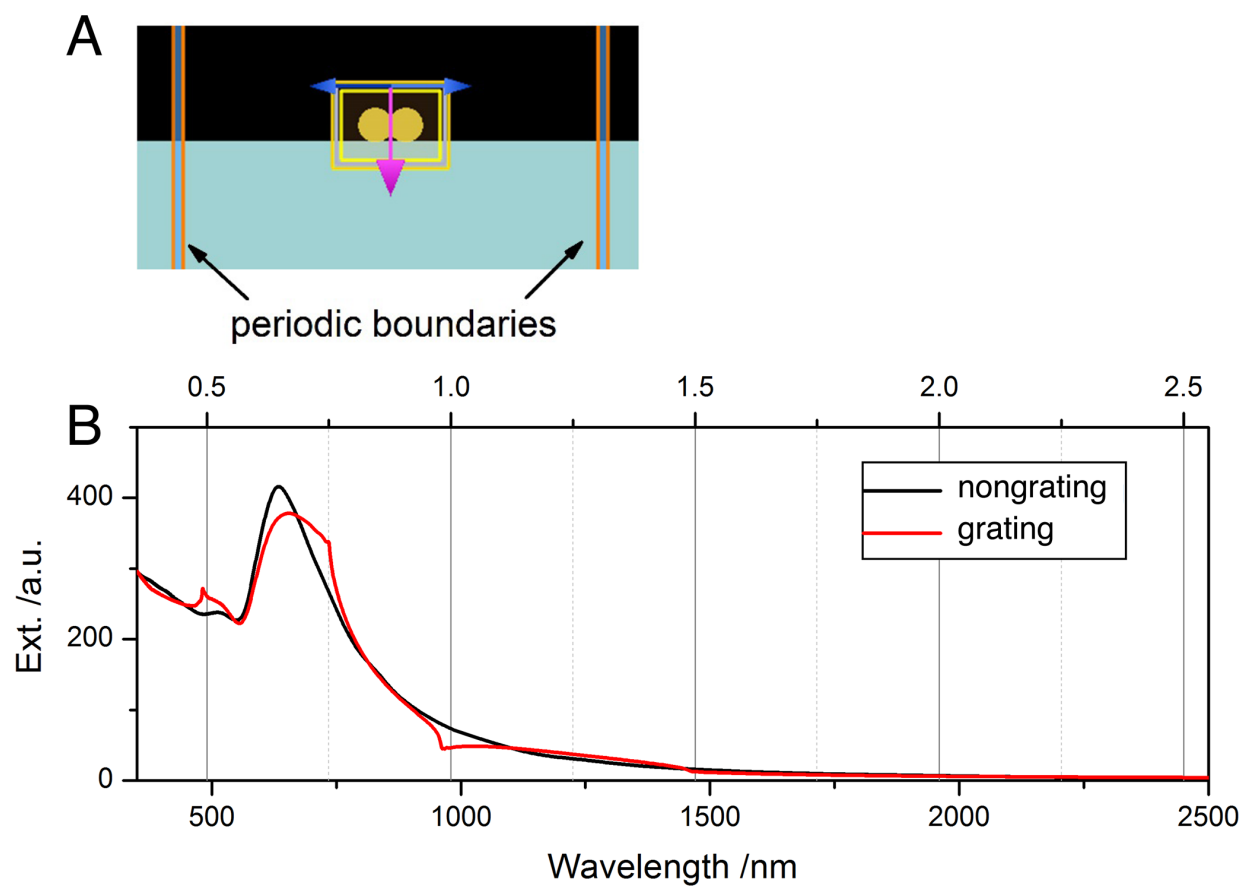


Figure S11. Two-dimensional modeling by FDTD of the grating effects (in transversal polarization) caused by periodic boundary conditions (A) shows changes of the extinction cross section (B) that are most pronounced at harmonics of the grating (λ/d).

REFERENCES

- (1) Jana, N. R.; Gearheart, L.; Murphy, C. J. *Langmuir* **2001**, *17*, 6782–6786.
- (2) Jana, N. R.; Gearheart, L.; Murphy, C. J. *J. Phys. Chem. B* **2001**, *105*, 4065–4067.
- (3) Pazos-Perez, N.; Garcia de Abajo, F. J.; Fery, A.; Alvarez-Puebla, R. A. *Langmuir* **2012**, *28*, 8909–8914.
- (4) Strozyk, M. S.; Chanana, M.; Pastoriza-Santos, I.; Pérez-Juste, J.; Liz-Marzán, L. M. *Adv. Funct. Mater.* **2012**, *22*, 1436–1444.
- (5) Genzer, J.; Groenewold, J. *Soft Matter* **2006**, *2*, 310–323.
- (6) Necas, D.; Klapetek, P. *Cent. Eur. J. Phys.* **2012**, *10*, 181–188.
- (7) Johnson, P. B.; Christy, R. W. *Phys. Rev. B* **1972**, *6*, 4370–4379.
- (8) Mie, G. *Ann. Phys.* **1908**, *330*, 377–445.
- (9) Gouesbet, G.; Grehan, G. *J. Opt. A: Pure Appl. Opt.* **1999**, *1*, 706–712.
- (10) Xu, Y. *Appl. Opt.* **1995**, *34*, 4573–4588.
- (11) Xu, Y. *Appl. Opt.* **1998**, *37*, 6494–6494.
- (12) Xu, Y. *Appl. Opt.* **1997**, *36*, 9496–9508.
- (13) Xu, Y.; Gustafson, B. A. S. *Astrophys. J.* **1999**, *513*, 894–909.
- (14) Ringler, M. *Ph.D. Dissertation, Ludwig-Maximilians-Universität München* **2008**.
- (15) Ringler, M.; Schwemer, A.; Wunderlich, M.; Nichtl, A.; Kürzinger, K.; Klar, T. A.; Feldmann, J. *Phys. Rev. Lett.* **2008**, *100*, 203002.